Available online at www.sciencedirect.com
ScienceDirect
Earth and Planetary Science Letters 257 (2007) 609–621
EPSL
www.elsevier.com/locate/epsl

High-temperature lithium isotope fractionation: Insights from lithium isotope diffusion in magmatic systems

Ian J. Parkinson *, Samantha J. Hammond, Rachael H. James, Nick W. Rogers

Department of Earth Sciences, The Open University, Walton Hall, Milton Keynes, MK7 6AA, UK

Received 4 July 2006; received in revised form 8 March 2007; accepted 12 March 2007
Available online 19 March 2007
Editor: R.W. Carlson

Abstract

Ion-microprobe analyses of the Li concentration and Li isotopic composition of zoned clinopyroxene and olivine phenocrysts from within primitive arc lavas from the New Georgia Group in the Solomon Islands reveal that both Li and δ^7Li vary widely from rim to core. The Li content of the rims is between 2 and 8 times that of the cores whereas Li isotope profiles are characterised by a zone with low δ^7Li (as low as −20‰) and cores with δ^7Li values of between −4 and +8‰; these over-print macroscopic major element zoning. With time, the low δ^7Li zone broadens and migrates towards the centre of the crystal and the Li concentration gradient is reduced. These data are consistent with preferential diffusion of ^{6}Li into the grain from a Li-enriched rim with ^{6}Li diffusing ~3% faster than ^{7}Li.

The profiles of δ^7Li and Li concentration can be reproduced by numerical modelling which confirms that the size of the δ^7Li trough is a function of the Li concentration gradient and the fractional difference in the diffusion rates of ^{6}Li and ^{7}Li. Both open and closed system models predict that a zone with low δ^7Li will migrate through the mineral grain with time, eventually relaxing back to a flat profile. Modelling of Fe-Mg diffusion in olivine suggests that the crystals have a residence time of 13–150 days, which is in accordance with the observed Li isotope profiles. This allows us to calibrate the rate of Li diffusion, which is 4–8 times slower in olivine and 20–30 times faster in clinopyroxene than Fe–Mg diffusion in olivine.

The high speed of Li diffusion means that the δ^7Li values of minerals that interact with Li-rich melts can rapidly decrease. Therefore, porphyritic lavas are unlikely to be suitable for Li isotope studies of mantle processes and it may also explain why olivines generally have higher δ^7Li than co-existing pyroxenes in some mantle samples. Modification of Li isotope ratios, by interaction with the host lava, may occur in mantle xenoliths during transport to the Earth's surface in only a few days. Conversely, melts ascending through the mantle will rapidly exchange Li and this may erase the pristine δ^7Li information that the melt carries. This may explain why many subduction zone lavas do not have an obvious slab signature. This study demonstrates that Li diffusion can overprint primary mineral compositions on very short timescales. This means that careful investigation of coexisting minerals is required, but it may also provide valuable information about the timescales of short duration events.

Keywords: Li isotopes; diffusion; isotope fractionation; subduction zone; magmatism

1. Introduction

Lithium is the lightest alkali metal and produces monovalent ions with small ionic radii. It has two isotopes, ^{6}Li

* Corresponding author. Tel.: +44 1908 659780; fax: +44 1908 655151.
E-mail address: I.J.Parkinson@open.ac.uk (I.J. Parkinson).

0012-821X/$ - see front matter © 2007 Elsevier B.V. All rights reserved.
doi:10.1016/j.epsl.2007.03.023

and ^{7}Li, which differ in mass by 16%. This mass difference produces significant variations in the ^{7}Li/^{6}Li ratio of up to 50 per mil (‰) at low temperatures [1,2]. Seawater has a rather homogeneous δ^{7}Li value of ~+31‰ ($\delta^{7}Li = [(^{7}Li/^{6}Li)_{sample}/(^{7}Li/^{6}Li)_{standard} - 1] \times 1000$, where the standard is the L-SVEC lithium carbonate [3]), whereas the upper continental crust has a δ^{7}Li value of between 0 and +2‰ [4]. During weathering ^{6}Li is preferentially retained in secondary minerals and soils can have δ^{7}Li values as low as −20‰ [1,4,5]. By contrast, mantle-derived basalts have a relatively homogenous composition, with δ^{7}Li values of 4±2‰ [1,6]. Hydrothermal alteration of both mid-ocean ridge basalts (MORB) and the underlying depleted peridotites produces material with δ^{7}Li values between 0 and +32‰ [7,8]. Recycling of material with such high δ^{7}Li into the mantle and subsequent mobilisation of Li from the slab is thought to be responsible for producing materials with high δ^{7}Li (+3 to +10‰) that have been reported for some subduction zone magmas [1,6,9].

Given the homogeneity of mantle-derived melts, it is perhaps surprising that mantle peridotites have a wide range in δ^{7}Li that extends to very low values. For example, clinopyroxene in mantle xenoliths from Japan and eastern Russia has δ^{7}Li values as low as −17‰ [10], while xenoliths from Zagarbad have δ^{7}Li values as high as +10‰ [11]. In the former study, those clinopyroxenes with very low δ^{7}Li also have very high Li contents (>30 ppm). This led the authors to propose that the mantle contains a Li-rich metasomatic component with very low δ^{7}Li (−40‰) that is equivalent to the EMII mantle component. Seitz et al. [12,13] have also reported temperature dependent partitioning of both Li and its isotopes between olivine and clinopyroxene; they observed that clinopyroxene has lower δ^{7}Li values than olivine, and that the size of this offset decreases with increasing equilibration temperature.

However, it is becoming increasingly clear that Li isotope ratios of mantle material may be affected by diffusion processes. The difference in the diffusion rates of two isotopes of an element is mass dependent and can be expressed as the ratio:

$$\frac{D_7}{D_6} = \left(\frac{m_6}{m_7}\right)^{\beta} \quad (1)$$

where D_6 and D_7 are the diffusion rates of lithium isotopes of masses m_6 and m_7 and β is an experimentally derived exponent [14]. Richter and co-workers [14,15] have conducted laboratory experiments that demonstrate significant physical kinetic isotope fractionation during diffusion in molten oxides and silicate melts. For example, an experiment utilising a basalt–rhyolite diffusion couple produced striking variations in δ^{7}Li values across the diffusion profile (of up to 40‰) and isotope compositions that are significantly different from the starting compositions [14]. This experiment produced a value for β of 0.215, indicating that ^{6}Li diffuses ~3.35% faster than ^{7}Li (Eq. (1); [14]). High-temperature Li isotope fractionation has also been documented in natural samples; peridotites close to melt conduits in the Trinity ophiolite show shifts in δ^{7}Li of up to 20‰ [16]. Furthermore, large variations in δ^{7}Li (of up to 50‰) have been recorded in single pyroxene grains in both nakhlite meteorites [17] and mantle xenoliths from San Carlos [18]. Both been attributed to differences in the diffusion rates of ^{6}Li and ^{7}Li. Finally, differences in the Li isotopic composition of coexisting olivine and clinopyroxene grains in mantle xenoliths from Tanzania and Eastern Russian have been attributed to melt/mantle interaction and Li diffusion [19,20]. Although diffusion profiles of δ^{7}Li will relax over time, the large shifts that have been observed in ^{7}Li/^{6}Li suggest that diffusion at magmatic temperatures is a viable mechanism for generating a wide spectrum of ^{7}Li/^{6}Li ratios in mantle-derived melts. Diffusion will occur, for example, during crystal growth in a magma chamber, during mantle-melt interaction, during partial melting and during melt transfer and magma mixing. Experimentally determined Li diffusion rates are very high in both melts [14,21] and silicate minerals [22,23] relative to other cations, and so Li isotopic fractionation by diffusion occurs over short timescales.

Here, we document some compelling examples of lithium isotope diffusion recorded in lavas from the New Georgia Group (NGG) in the western Solomon Islands. Our data confirm differential diffusion of lithium isotopes in silicate minerals and allow us to estimate diffusion rates of lithium in olivine and clinopyroxene. Such information is crucial for assessing timescales of magmatic processes. We also report the results of numerical modelling of diffusion profiles in mineral grains that provide a theoretical basis for understanding both our new data and also for interpreting Li isotope variations in mantle and volcanic rocks in general.

2. Geological setting and sample description

The NGG lavas are part of a suite of primitive arc lavas that erupted in the last 3–8 million years in response to the subduction of the Woodlark Basin (and spreading-centre) beneath the Pacific plate [24]. Picritic

and ankaramitic lavas are the dominant volcanic product [25–27] and were chosen as a suitable suite of lavas to study Li isotope systematics in subduction zones because of their primitive whole-rock chemistry and simple mineralogy. However, some lavas have up to 30% phenocrysts and this means that the whole-rock chemistry is not simply related to any erupted magma composition (see also [27]). Petrographically, large clinopyroxene (1–3 mm) and olivine (0.5–1 mm) crystals dominate the phenocryst assemblage. The groundmass is holocrystalline and consists of small (<50 μm) clinopyroxene, oxide and plagioclase crystals. Clinopyroxene grains are macroscopically zoned with respect to major elements and olivine grains have iron-rich rims (see Fig. 1). During routine laser ablation inductively coupled plasma mass spectrometry (ICP-MS) studies we also discovered significant Li zoning within the clinopyroxene grains; the rims of the grains had up to 8 times the Li concentration of the cores. The rims also had rare earth element (REE) patterns that were distinct from the cores, indicating crustal contamination during the final stage of the crystallisation process [28]. To help interpret the enigmatic Li isotope data that we had obtained on whole-rock samples, we therefore decided to undertake a high-resolution ion-microprobe study of the Li isotope composition of these zoned clinopyroxenes. Some of these Li isotope data are presented below; a more detailed study of the geochemistry of the NGG lavas will be presented elsewhere.

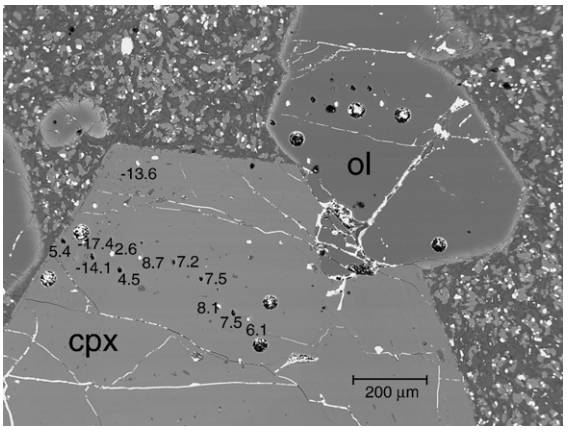

Fig. 1. BSE image of coexisting clinopyroxene and olivine grains within sample 95.11.14.10. Numbers represent measured δ^7Li values (see supplementary data). Note the well-developed Fe-rich (brighter) rims on the olivine and the very narrow rim zone of the clinopyroxene. Smaller pits are from ion-probe analyses whereas the larger holes are from LA-ICP-MS analyses. One point with a δ^7Li value of −13.6 was determined away from the main traverse, but plots correctly on the profile in Fig. 3b.

3. Analytical techniques

3.1. Electron microprobe analyses

Minerals were analysed for major and minor elements using a Cameca SX100 electron microprobe (EMP) at the Department of Earth Sciences, The Open University using a 10 μm spot with operating conditions of 20 nA and 20 kV and calibrated using natural mineral standards. Traverses across the mineral grains were made using a 1 μm spot size and 2–3 μm spacing. An olivine standard not used in the primary calibration reproduced with a forsterite content of 0.9089±0.0010 which is within error of the published value of 0.9088 [29] and considerably less than the variation recorded in the NGG lavas (0.68–0.86). BSE images were generated using a 1 μm spot size to illustrate the zoning within clinopyroxene and olivine grains (see Fig. 1).

3.2. Ion-microprobe analyses

Clinopyroxene and olivine grains, that had previously been analysed by electron microprobe and laser-ablation ICP-MS, were analysed for both lithium concentrations and isotope composition using a single-collector secondary ion mass spectrometer (SIMS) (Cameca ims 4f) at the NERC ion-microprobe facility at the University of Edinburgh. Full details of the analytical technique are given in [30]. Briefly, positive secondary ions ($^6Li^+$, $^7Li^+$) were produced by a $^{16}O^-$ 40 nA primary beam focused to a 30 μm spot size with a net impact energy of 14.5 keV. The secondary ions were analysed with an energy window of 52 eV, a 150 μm image field using the 400 μm contrast and the 1800 μm field apertures. The Li isotope ratios were measured for 100 cycles on the electron multiplier, each cycle consisting of 5 and 2 s count times on $^6Li^+$and $^7Li^+$, respectively. Li isotope ratios are determined on a 20–30 μm diameter spot and the $^7Li/^6Li$ ratio of the mineral is referenced to the glass standard BCR-2 g (that has δ^7Li=4.08±1.00 [30]), which is measured several times during each analytical session. The external error of this standard was ±1.2‰ (2σ, where σ is the standard deviation) over the course of this study. Lithium concentrations were normalized to NIST SRM 610 and calculated from the measured $^7Li^+/^{30}Si^+$ ratio, the SiO_2 content and an empirical correction factor [30]. The external error of the lithium concentration measurements was less than 6% (2σ) during the course of this study.

Channon et al. [31] have recently demonstrated matrix dependent effects on SIMS (Cameca 5f) analyses of

Li isotope ratios in olivine, with ~1.3‰ shifts in δ^7Li per 1 mol% change in forsterite. This effect has not been documented on other ion-microprobes [R. Hervig personal communication]. Although we cannot completely rule out a matrix effect on our olivine analyses, the relative δ^7Li of only one of our olivine analyses would be effected. This point would still be at least 4‰ lighter than the core composition of the olivine and would not effect the conclusions we draw from our olivine data (see Fig. 3a). We have also analysed a number of homogeneous mantle clinopyroxene and olivine grains by SIMS and multi-collector ICP-MS and they have the same δ^7Li values (within analytical uncertainty) [28]. A similar conclusion was reached by [18], but they noted that there may be ~2‰ disparity between olivine analysed by SIMS and MC-ICP-MS. We are confident that the Li isotopic profiles for clinopyroxene are accurate because no matrix dependent effects have been discovered for clinopyroxene [R. Hervig personal communication] or in previous studies [8,18,28]. Furthermore, our Li isotopic profiles overprint the major element zoning in the NGG clinopyroxene crystals.

4. Results

Major element, lithium and lithium isotope data are presented for three individual clinopyroxene grains and one olivine grain from three different NGG lavas (95.11.14.10, 95.11.13.8 and 95.11.13.9) in Figs. 1, 2 and 3. These samples were selected on the basis that they span the range of patterns of Li and Li isotope profiles observed in all of the NGG lavas that we have analysed to date.

4.1. Major element data

The BSE image in Fig. 1 is for lava 95.11.14.10 and illustrates some characteristic features of the clinopyroxene and olivine grains in the NGG lavas. The clinopyroxenes have complex oscillatory zoning but very narrow Fe-rich rims (this is difficult see in Fig. 1). The clinopyroxenes are ferric-iron rich with $Fe^{3+}/\Sigma Fe$ ratios of 0.38–0.46 (based on stoichiometry), consistent with the elevated oxygen fugacities recorded in the lavas [27]. Taking into account the ferric iron, the outer rim zones are diopside in composition with $Ca_{47}Mg_{46}Fe_7$, whereas the very narrow Fe-rich rim is salitic in composition ($Ca_{46}Mg_{44}Fe_{10}$). Careful electron probing of the rim using a 1 μm diameter spot reveals that this zone is only ~1 μm thick; it has a Mg# of 0.83, whereas the rest of the rim zone has a Mg# of 0.87. The outer rim is also enriched in TiO_2 (0.53 versus ~0.4 wt.%) and very depleted in Cr_2O_3 (0.03 versus 0.35–0.4 wt.%) relative to the rim zone. This indicates that the outer rim crystallised from a much more evolved melt than the one that crystallised even the outer 20 μm of the clinopyroxene. Similar compositional variations have been found for clinopyroxenes in the other NGG lavas [28].

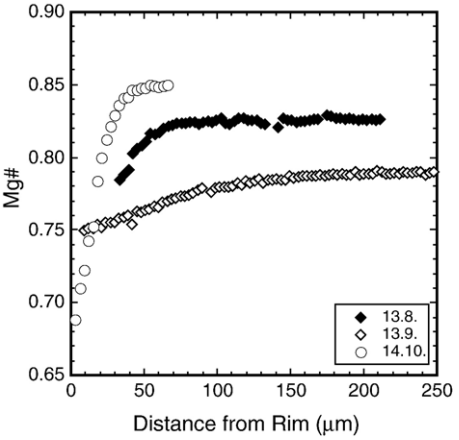

Fig. 2. Profiles of Mg# of olivine grains from each of three lavas analysed for Li isotopes. Each profile has a characteristic diffusion length-scale that is discussed in the text. There are few data close to the rim of sample 95.11.13.9 because small amounts of matrix material were analysed along with the olivine which compromises the olivine analyses.

By contrast, the olivines have wider Fe-rich rims that are amenable to detailed EMP traverses. Representative electron probe analyses of olivine grains from each of the three lavas are presented in Fig. 2. They reveal that the composition of the core of the olivines is variable (Mg# ranges from 0.79 to 0.85) and that each sample has equilibrated with a different melt; that is, the rims have estimated Mg#s of between 0.67 and 0.74. All of the olivines are high-Ca (>0.3 wt.% CaO) and do not exhibit a Ca diffusion profile (cf. [27]). Finally, it is clear that the data shown in Fig. 2 take the form of diffusion profiles and the profiles flatten out at different distances from the rim (45, 85 and 180 μm). Therefore the duration of final melt equilibration is different for each olivine and/or occurred at different temperatures. We will return to quantifying the diffusion timescales in Section 6.2, but a first order observation is that the residence time of individual olivine phenocrysts increases from sample 95.11.14.10 to 95.11.13.8 to 95.11.13.9.

4.2. Lithium and lithium isotope data

Fig. 3 shows profiles of δ^7Li and Li concentration for the three clinopyroxenes and the one olivine (these data

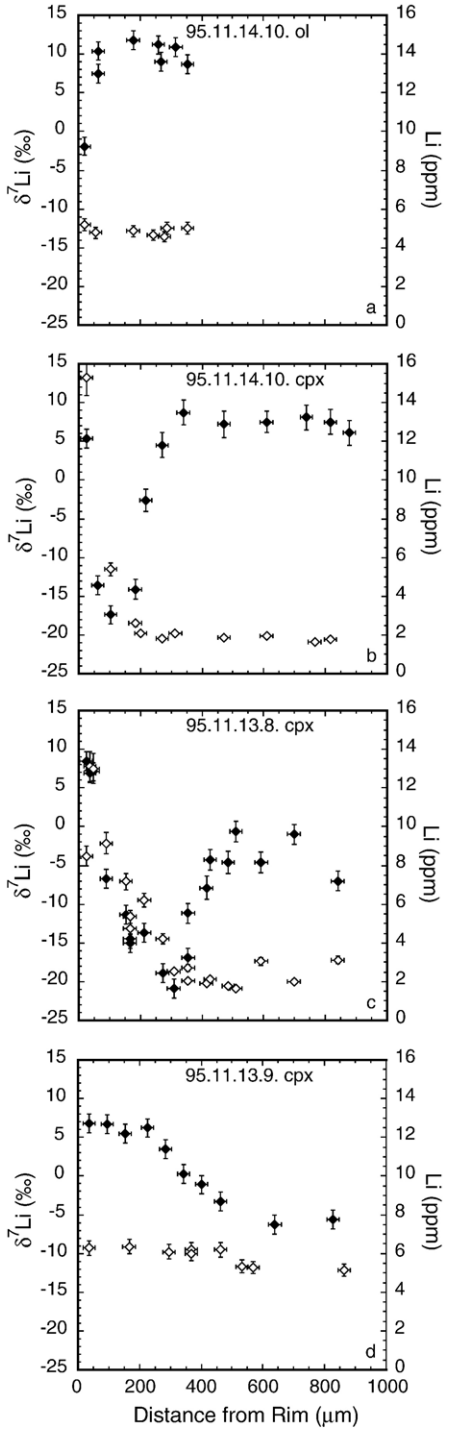

Fig. 3. Profiles of Li concentration (open diamonds) and δ^7Li (solid diamonds) versus distance for one olivine and three clinopyroxenes from the NGG lavas. Uncertainties are the 2σ external precision unless the 2 S.E. uncertainty was larger. The profiles are shown in order of increasing crystal residence time to illustrate their evolution with time.

are provided in the Supplementary Data). Distance from the rim of the grain is measured orthogonal to the crystal edge towards the core as identified from the BSE images. This measurement may not represent the true distance relative to the core in three-dimensions because the grains are randomly orientated within the thin section. However, we chose large grains which, in the case of the clinopyroxenes have basal section shapes, so that they are likely to have been cut approximately orthogonal to the *c*-axis. However, it is difficult to assess whether any of the traverses cross the true core of the mineral in three dimensions. We address this issue in Section 5.

Data for the olivine crystal in lava 95.11.14.10 are shown in Fig. 3a. Li concentrations show little variation across the crystal (ranging from 4.6 to 5.0 ppm) although the concentration at 19 μm from the rim is slightly higher (5.2 ppm). The δ^7Li value of the spot located 19 μm from the rim is −1.9‰, whilst the interior of the crystal (65–353 μm) has higher δ^7Li (10±1.5‰).

Data for the clinopyroxene crystal in this same lava are presented in Fig. 3b. Li concentrations are relatively constant in the innermost 700 μm of the grain (1.9± 0.3 ppm) but increase sharply towards the rim, reaching a value of 15.3 ppm at 26 μm from the rim. The Li isotope profile has a trough with a minimum δ^7Li value of −17.4‰ at 104 μm from the grain edge. Close to the rim, δ^7Li increases to 5.4‰ and the core of the mineral (>330 μm) has relatively constant δ^7Li (+7±1‰). Thus, the δ^7Li profile is decoupled from the Li concentration profile and it transcends several of the major element zones (Fig. 1).

Three separate rim-to-core traverses, each starting at a different grain edge, were obtained for a single clinopyroxene grain from lava 95.11.13.8. These data have been combined in Fig. 3c. The combined Li concentration profile takes the form of a smooth curve with values decreasing from ~13 ppm at 30 μm from the rim to 2–3 ppm between 450 μm and the core. The combined δ^7Li profile again shows a trough; this is located further into the crystal (~300 μm) and it has a lower minimum δ^7Li value (−20.9‰). The high density of data obtained for this mineral grain (15 points over a distance of 450 μm, from three separate traverses) defines the δ^7Li trough extremely well and suggests that Li diffusion rates are not strongly dependent on crystallographic orientation.

The final clinopyroxene grain, from lava 95.11.13.9, shows very little change in Li concentration. Values are ~6.3 ppm at the rim and ~5.2 ppm in the core of the grain (Fig. 3d). There is rather more variation in δ^7Li, but

no pronounced trough. δ^7Li values are around +6±1‰ within 200 μm of the rim, and they gradually fall to values of around −6‰ in the core of the grain.

5. Numerical modelling

In order to understand the form of the Li and Li isotope profiles that we have observed in these mineral grains, to calibrate lithium diffusion rates and to make some predictions about the behaviour of Li and its isotopes in magmatic systems, we have undertaken some numerical modelling. Our approach is similar to that of [17], who also looked at Li exchange between individual mineral grains surrounded by a melt phase. This process can be described using a version of Fick's second law for radial diffusion within a sphere:

$$\frac{\partial C^{n\mathrm{Li}}}{\partial t} = D^{n\mathrm{Li}}\left(\frac{\partial^2 C^{n\mathrm{Li}}}{\partial r^2} + \frac{2}{r}\frac{\partial C^{n\mathrm{Li}}}{\partial r}\right) \quad (2)$$

In this equation, ^{n}Li is either ^{6}Li or ^{7}Li, $C^{n\mathrm{Li}}$ is the concentration of a lithium isotope (at t and r), $D^{n\mathrm{Li}}$ is the diffusion rate of a lithium isotope, r is the radial distance from the centre of the grain and t is time [32]. Eq. (2) has analytical solutions for simplified boundary conditions, but it can also be solved numerically by various finite-difference methods [32–34]. Here, we use an explicit finite-difference method (e.g., [33]) as it is both simple to program and amenable to varying the boundary conditions and initial compositions. One problem with this method is that it can develop composition oscillations with exponentially expanding errors if the time step (Δt) is too large; solutions are only stable when s, a measure of the solution stability, is less than 0.5. s is defined by:

$$s = \frac{D^{n\mathrm{Li}}\Delta t}{\Delta r^2} \quad (3)$$

where Δr is the radial grid spacing (see [33]). Finite-difference methods produce simulations whose accuracy increases as Δt decreases so our model has to be tailored to the required accuracy. We use a 10 μm grid and a time step that reproduces ^{7}Li/^{6}Li ratios to better than 0.1‰ relative to the analytical solution to the diffusion equations for simplified models [33]. As ^{6}Li and ^{7}Li have very different diffusion rates, the two isotopes must be effectively treated as two elements, so two parallel diffusion calculations are performed and the data are combined to produce ^{7}Li/^{6}Li ratios and Li mass balance (see also [16,17]). δ^7Li values are calculated relative to a ^{7}Li/^{6}Li ratio of 12.333.

Most of the Li and Li isotope data reported in the literature for individual mineral phases are for the whole mineral grain and thus represent the average [10,12,20]; spatially resolved ion-probe data are still relatively unusual [17,18]. The average Li concentration and δ^7Li value of a mineral at any given time can be obtained from our model by evaluating the integral:

$$\int_0^R 4\pi r^2 C^{n\mathrm{Li}} dr \quad (4)$$

where $C^{n\mathrm{Li}}$ is the concentration of a lithium isotope at some point within the mineral grain and R is the radius of the mineral.

5.1. Model results

The most striking feature of the Li isotope profiles shown in Fig. 3 is the presence of extremely low δ^7Li values quite unlike the values recorded in whole-rock measurements of mantle-derived material. This is a natural consequence of the different diffusion rates of ^{6}Li and ^{7}Li as they diffuse along a concentration gradient. However, the minimum value of the isotopic trough is a non-steady state feature and it will evolve with time. The significance of this for geological processes is discussed in the next section, but it is worthwhile first to explore what controls the magnitude of the isotopic shifts.

Richter et al. [14] demonstrate that the value of the δ^7Li minima is a function of the concentration gradient and the difference in the diffusion rates of ^{6}Li and ^{7}Li (effectively a fractionation factor, f). The effects of this are shown in Fig. 4: C_S/C_0 is the ratio of the concentration at the mineral surface (i.e. in equilibrium with the melt) relative to the initial concentration in the mineral grain and the ratio of the ^{6}Li/^{7}Li diffusion rates (i.e. D_7/D_6 in Eq. (1)). The curves shown in Fig. 4 represent the 'instantaneous' fractionation that occurs due to differential diffusion. As will be shown below, the minimum δ^7Li value of the trough decreases with time as the trough migrates across the grain in a sphere and the composition of the whole-grain also drops to a minimum.

The key result is that any process in which the mineral surface has a higher Li concentration than the mineral interior will generate low δ^7Li values in the mineral, even if there is no difference between the initial Li isotope composition of the surface (i.e. the melt) and the mineral interior. In the case of an open-system model, the whole grain will also have a very low δ^7Li value although this will, over time, return to the isotope

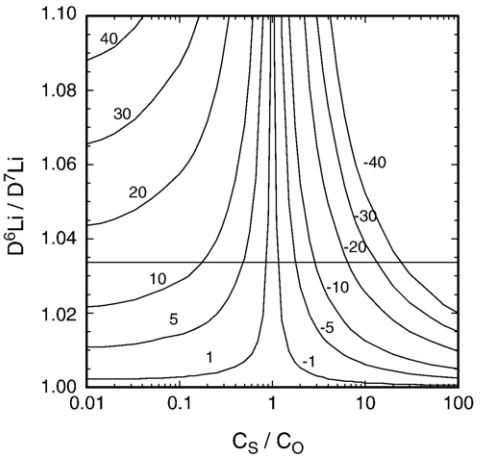

Fig. 4. Plot of C_S/C_0, the ratio of the concentration at the mineral surface to that in the mineral interior, versus the ratio of the diffusion rates of ^{6}Li and ^{7}Li. The graph is contoured with respect to the δ^7Li minimum (or maximum) that is generated 'instantaneously' due to diffusion-driven isotope fractionation. The horizontal line represents the experimentally derived ratio for the two lithium isotopes [14]. Any process that produces an elevated Li concentration at the surface of the mineral generates a δ^7Li trough whereas any process that produces low Li concentrations at the surface gives a δ^7Li peak. The curves will be displaced progressively to the left during diffusion within a sphere and this effect needs to be taken into account when estimating the ratio of the diffusion rates of ^{6}Li and ^{7}Li from natural samples (see text).

composition of the melt. On the other hand, if the mineral surface has lower Li than the mineral interior, ^{6}Li will diffuse out of the mineral faster than ^{7}Li generating regions within the mineral with high δ^7Li.

5.1.1. Open-system model

In an open-system, the mineral surface maintains a constant Li concentration (and isotope composition). This is likely to be the case for a phenocryst equilibrating in a magma chamber or a mantle mineral that is equilibrating with a migrating melt that is constantly replenished. Fig. 5 shows the results of such a model for a grain of radius 1 mm and the results are similar to those presented by [17]. The position of the δ^7Li trough moves from close to the rim to the core of the mineral over time and the minimum δ^7Li value of the trough also decreases (because of the spherical geometry). By the time the edge of the trough has reached the core of the grain, the δ^7Li value of the core has fallen to −53‰ (in this example). Note that the grain then recovers its original lithium isotopic composition, producing a δ^7Li profile that looks like a conventional diffusion profile. It has already been noted that Li diffuses rapidly in silicate minerals, [16,22,23]. In this example, which adopts a ^{7}Li diffusion rate of 1×10^{-11} cm^2 s^{-1}, the grain completely equilibrates with the mineral surface in ~25 yr. This diffusion rate was selected because, as we demonstrate later in this paper, it is appropriate for the clinopyroxene crystals in the NGG lavas.

This calculation highlights some key features about the modification of a mineral grain during diffusive exchange of Li isotopes. Firstly, on encountering a melt, the core only retains its original composition for a short period of time; for this model with a grain radius of 1 mm, about 250 days. Secondly, while the rim of the grain has a δ^7Li value that is equal to that of the surface contaminant, the δ^7Li value only 20 μm in from the rim may be lower by 2 to 5‰, even after a few days of diffusional exchange. Therefore it is important to ion-probe to within 10 μm of the grain boundary to obtain compositional information about the melt phase.

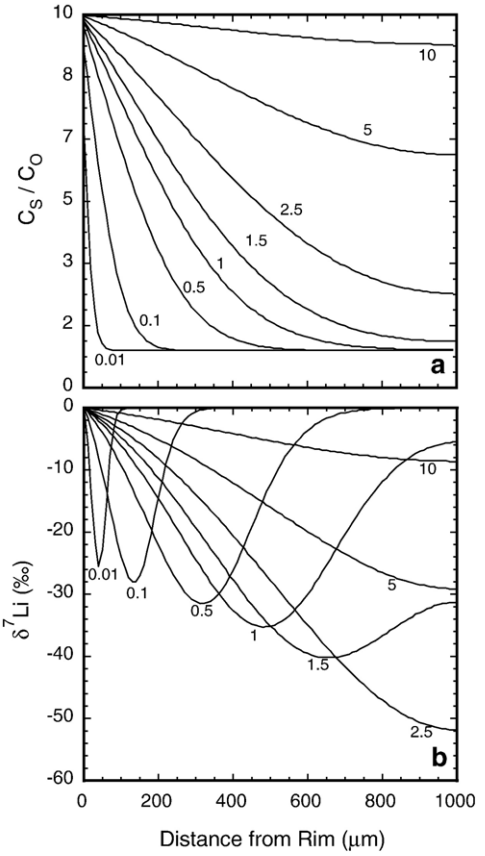

Fig. 5. Results of an open-system numerical model in which: the Li content at the mineral surface is 10 times that of the initial mineral (C_S/C_0, = 10); the isotope composition of the mineral surface and interior is the same (δ^7Li=0); the diffusion rate of ^{7}Li is 10^{-11} cm^2 s^{-1} and the diffusion rate of ^{6}Li is 1.0335×10^{-11} cm^2 s^{-1} [14]. (a) Evolution of the total Li concentration with time (numbers on the figure are in years); (b) evolution of δ^7Li.

One further aspect of open-system behaviour is illustrated in Fig. 6. This shows the variation in the δ^7Li value of the whole mineral grain over time as it interacts with a melt/fluid phase that is enriched in Li (as expressed by the C_S/C_0 ratio). This would apply to, for example, mantle peridotites undergoing melt reaction. For any given C_S/C_0 ratio, mineral δ^7Li values rapidly decrease before recovering to the δ^7Li value and concentration of the grain boundary. What is striking is that the δ^7Li value of the grain can shift dramatically with only a small change in the C_S/C_0 ratio. The open circles on Fig. 6 show the effect of only 1 day of interaction; note that large shifts in δ^7Li values can be produced particularly for $C_S/C_0 > 10$. The change in δ^7Li in peridotite minerals will depend on their Li diffusion rate and the whole-rock δ^7Li value will reflect the modal mineralogy of the peridotite and the diffusional timescale.

5.1.2. Closed-system model

In a closed-system, a rim grows instantaneously (in this example 100 μm wide) such that it has a higher Li concentration than the original grain. The step-like Li profile is then allowed to diffusively equilibrate without further addition of Li. This model is applicable to slowly cooling mantle or cumulate rocks, which may finally equilibrate in a closed-system. Profiles of Li and δ^7Li generated by such a model are shown in Fig. 7. With time, the δ^7Li profile evolves in a similar fashion to that of the open-system model except that rim zone initially

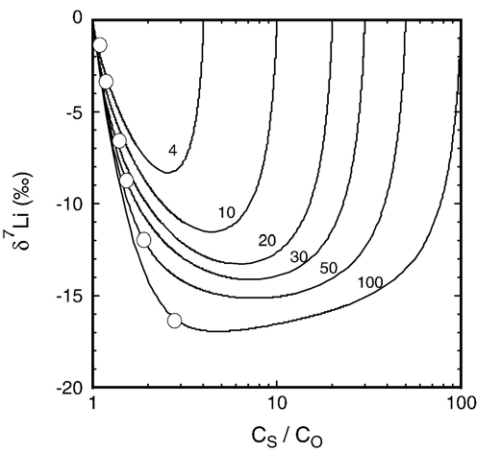

Fig. 6. Evolution of the Li concentration (expressed as a function of C_S/C_0) and δ^7Li in a whole grain undergoing open-system interaction for diffusion rates of 10^{-11} cm^2 s^{-1} for ^{7}Li and 1.0335×10^{-11} cm^2 s^{-1} for ^{6}Li [14]. The curves are for C_S/C_0=4, 10, 20, 30, 50 and 100. The parabolic trajectories define the evolution of the whole grain until it recovers back to δ^7Li=0. Open circles represent composition reached after only one day of interaction for each curve (see text).

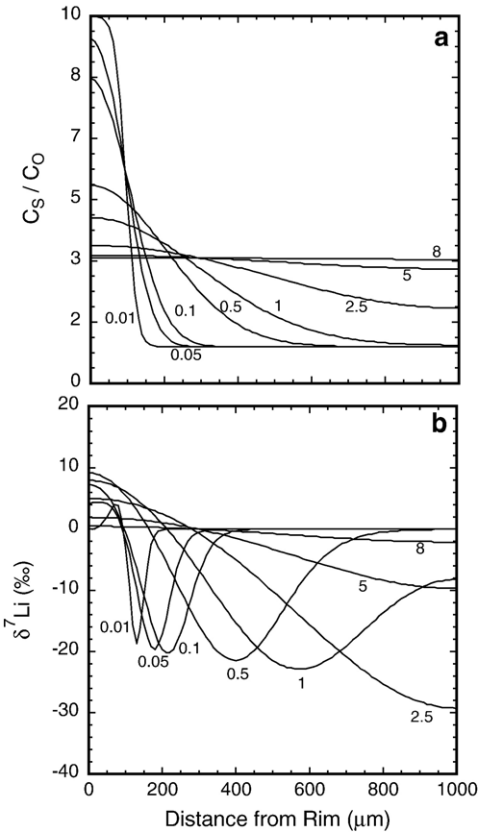

Fig. 7. Results of closed-system numerical model in which a zone 100 μm thick grows instantaneously with a concentration 10 times that of the initial mineral composition (C_S/C_0,=10) and the total Li concentration of the new grain is then kept constant. All other parameters are the same as Fig. 5. (a) Evolution of the total Li concentration with time (numbers on the figure are in years), (b) evolution of δ^7Li.

acquires higher δ^7Li because it becomes depleted in ^{6}Li. The δ^7Li value of the rim can be as much as +10‰ higher than the δ^7Li value of the melt phase. Nevertheless, the isotopic composition of the whole grain must, by definition, remain constant.

5.1.3. Effects of grain geometry

Grain geometry plays an important role in quantifying diffusion timescales because diffusion of all cations varies with crystallographic direction. As noted in Section 4.1, it is not clear whether our Li profiles traverse the centre of the grains, although the similarity between the shapes of the measured profiles and the numerical models suggests that we have sampled representative portions. This is also supported by multiple traverses across a single grain (Fig. 3e and f) that combine to produce a consistent δ^7Li profile. The effects of missing the grain centre on a δ^7Li profile are

shown in Fig. 8a. The further the traverse lies from the centre of the sphere, the more 'relaxed' the profile appears such that it looks like it has been produced over a longer period of time (see Fig. 5b). Minimum δ^7Li values may also be missed. The effects of grain geometry thus have important implications for the correct interpretation of Li diffusion profiles. A simple practical approach is to check the size of the phenocrysts in hand-specimen and to make sure the ion-microprobe traverses are of similar length as slicing a grain further away from the centre produces increasingly shorter traverses (see Fig. 8a). In the case of clinopyroxene phenocrysts, which have 8-sided basal sections, it is thus perfectly possible to choose a suitable crystal.

However, pyroxenes in mantle peridotites often have plastically deformed textures and basal sections are rarely found. For a rectangular pyroxene crystal the core is represented by a line through the centre of the crystal. If the crystal is sliced across the basal section then a δ^7Li profile similar to that shown in Fig. 8a is produced. The effects of slicing the crystal parallel to its centre are shown in Fig. 8b. Again, missing the core region can generate δ^7Li profiles that are very different from the 'true' profile but, in this example, the minimum δ^7Li value is always measured. Profiles similar to those shown in Fig. 8b have been reported for mantle orthopyroxene [18]; these would be difficult to model without knowing the position of the ion-microprobe traverse relative to the mineral core.

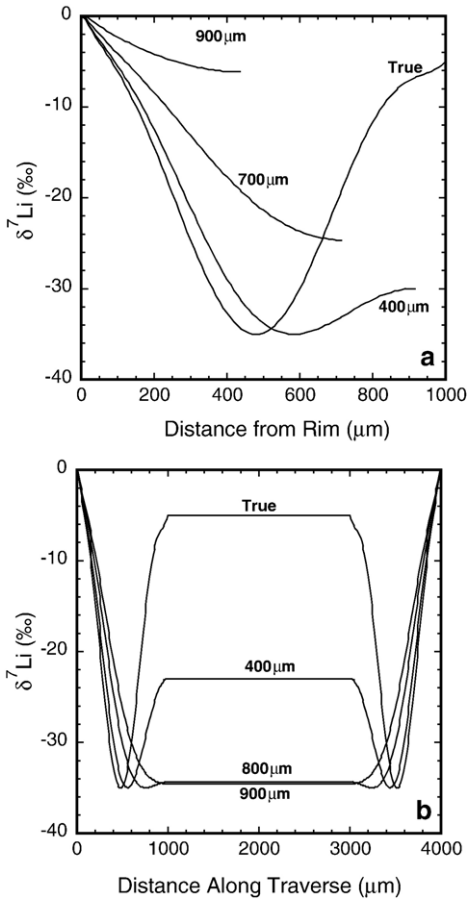

Fig. 8. (a) Profile of δ^7Li in a spherical geometry that has been sliced at different (0, 400, 700 and 900 μm) distances from the grain centre. The profile labelled 'True' has been sliced through the grain centre (0 μm). (b) Profile of δ^7Li in a rectangular geometry for the long axis of a mineral (e.g., pyroxene) that has been sliced at different (0, 400, 800 and 900 μm) distances from the diffusion centre (see text for details).

6. Discussion

6.1. General observations

The shapes of the Li isotopic and concentration profiles that we have measured in the NGG clinopyroxenes are very similar to those produced by our numerical modelling of open-system Li diffusion. The relative rates of ^{7}Li and ^{6}Li diffusion can be calculated because we have measured both the Li concentration of the melt and the mineral core and the minimum δ^7Li value for several clinopyroxene grains (see Fig. 4a). This calculation yields a fractionation factor of between 1.029 and 1.042 which corresponds to a β value of 0.19–0.27 in Eq. (1). This range overlaps with the value of 0.215 derived by [14], indicating the there may be little difference in the behaviour of Li isotopes during diffusion in silicate melts and minerals.

If we know the Li diffusion rate, then we can calculate the timescale over which the ion-microprobe profiles were produced; this in turn allows us to estimate the residence time of the crystals prior to eruption. We can also calculate the crystal residence times from the Fe-Mg diffusion profiles.

6.2. Quantifying crystal residence times

The petrography and petrology of the NGV lavas indicate that although they have primitive whole-rock chemistries, most of the lavas are actually a mixture of relatively primitive phenocrysts in a more evolved matrix. The low Mg# of the rims of the olivine and clinopyroxene grains indicates that they may have only coexisted in a low MgO melt just prior to eruption; in this regard, we note that the Fe-rich rims in the clinopyroxenes are very narrow, but they are broader in the olivines (Fig. 1).

The Fe–Mg profiles allow us to quantify the absolute diffusion rates in olivine and clinopyroxene. The

diffusion profiles are narrow relative to the size of the phenocrysts so they can be fitted using a one-dimensional semi-infinite media equation:

$$\frac{C_x - C_S}{C_0 - C_S} = \mathrm{erf}\left(\frac{x}{2\sqrt{Dt}}\right) \quad (5)$$

where C_x is the concentration at distance x from the surface at any given time, C_0 is the concentration at 'infinite' depth in the crystal, C_S is the concentration at the surface of the crystal, x is the depth into the crystal, D is the diffusion coefficient, t is time and erf is the error function [32]. Fitting of the data is accomplished by plotting x against the inverse of the error function of $(C_S - C_x)/(C_S - C_0)$ which gives a straight line with a slope of $(4Dt)^{-0.5}$super $^{0.5}$ and an intercept of 0. C_0 is varied until the intercept is equal to 0 and the straight line is fitted using least-squares methods [35]. This method also allows the rim composition to computed when it was not possible to measure by EMP. Results of the modelling for the three olivine crystals are that the Mg of the rim is 0.701±4, 0.744±4 and 0.650±4 and the slope $(4Dt)^{-0.5}$super $^{0.5}$ is 203±18, 77.8±3.9 and 385±24 for lavas 95.11.13.8, 95.11.13.9 and 95.11.14.10, respectively.

In order to derive the time required to produce the diffusion profile, we need to know the diffusion rate and therefore the temperature. We use the Fe–Mg exchange diffusion rate parallel to the c-axis for olivine of [36] that was parameterised by [37]:

$$D_{\mathrm{Fe-Mg-ol}} = 8 \times 10^{-3} \exp\left(\frac{247}{RT}\right) \quad (6)$$

where R is the gas constant and T is the temperature in Kelvin. There is considerable variation in the published Fe–Mg exchange diffusion rates that depend strongly on oxygen fugacity [37,38] and less strongly on crystallographic direction [36]. We have chosen a diffusion rate appropriate for the oxidised NGG lavas, but there will be some additional uncertainty due to variations in the orientation of the olivine crystals we have analysed. The lack of glass in the matrix makes geothermometry of the lavas difficult. We have therefore calculated the temperature in two different ways. Firstly, we take the Mg of the rim of the olivine and calculate the Mg# of the equilibrium melt using a partition coefficient for Fe-Mg exchange of 0.3 [39]. This value does not represent the equilibrium value for the whole rock because of cumulus olivine enrichment. A plot of Mg# versus MgO for the whole rock data from the NGG suite (IJP unpublished data), however, enables us to estimate the MgO content of the matrix (melt), an approach used by other workers to derive primitive melt compositions [40]. The Mg# of the whole-rock takes into account the high fO_2 of the NGG lavas which is 1–2 log units above the Fayalite–Magnetite–Quarz (FMQ) buffer ([27], IJP unpublished data) using the parameterisation of [41]. From the MgO content (2.0–4.5 wt.%) we calculate the temperature using the thermometer of [42] which yields a temperature of 1050 °C for 95.11.14.10, 1075 °C for 95.11.13.8 and 1100 °C for 95.11.13.9. Secondly, we can use the olivine-clinopyroxene thermometer of [43] by utilising the rim compositions of the two minerals as they are likely to have been in equilibrium. This method yields comparable temperatures, as long as the Fe^{3+} content of the clinopyroxene is taken into account, and also generates a range in the lava temperatures of ~50 °C. These temperatures are lower than the primary magmatic liquid temperature for the NGG lavas calculated by [27] but comparable to olivine-spinel temperatures [27]. Our calculated temperatures yield residence times of 32.6±5.9, 149±15 and 13.8±1.4 days for 95.11.13.8, 95.11.13.9. and 95.11.14.10, respectively. These are in the range of residence times calculated from Fe–Mg and Ca diffusion in olivine in other NGG lavas [27]. It should be noted that diffusion–reaction experiments by [21] generated olivine with normal zoning (higher Mg# in the core), similar to what we observe, but without the need for lowering of the melt Mg#.

6.3. Li diffusion rates

There is a good correspondence between the olivine residence times and the Li isotope profiles in the clinopyroxene; the lava with the shortest residence time (95.11.14.10) has a narrow δ^7Li trough that lies close to the grain rim and the lava with longest residence time (95.11.13.9) has a broad δ^7Li trough. We can be confident that the Li isotope data relate to a diffusion event just prior to eruption. Coexisting clinopyroxene and olivine data in sample 95.11.14.10 allow us to calculate the relative rates of Li diffusion in these phases referenced to the Fe–Mg diffusion rate in olivine. The rates are essentially independent of temperature because the activation enthalpies for Li diffusion in clinopyroxene and Fe–Mg diffusion in olivine are very similar (258 versus 247 kJ mol^{-1} [23,37]). The position of the δ^7Li trough in the olivine (19 μm) and clinopyroxene (120 μm) allows us to calculate the relative diffusion rates using the diffusion model described previously. Li diffusion rates are 4–8 times slower, and 20–30 times faster, in olivine and

clinopyroxene, respectively, than for Fe–Mg diffusion in olivine. The value that we obtain for Li diffusion in clinopyroxene is ~500 times slower than that reported by [23]. However, the narrow (1 μm) Fe-rich rim of the clinopyroxene suggests a short residence time (tens of days) on the basis of Fe–Mg diffusion rates and recent studies of clinopyroxenes from Vesuvius [44]; this is consistent with our data and concurs with [18] who also infer slower Li diffusion rates in clinopyroxene than [23].

The discrepancy between our estimates for Li diffusion and the experimental studies of [23] may reflect a number of factors. These include the large difference in oxygen fugacity (3.2–0.9 log units lower than the FMQ buffer) for the experiments compared to 1–2 log units above the FMQ buffer for the NGG lavas. The NGG clinopyroxenes also have much higher ferric iron contents and lower Mg# than the experimental clinopyroxene [23]. Finally, the experimental clinopyroxenes from [23] are Li-rich (2% atoms per formula unit) and so self-diffusion may enhance the Li diffusion rate [17].

Our main conclusion from this section is that Li diffuses considerably faster in clinopyroxene than olivine, although the absolute diffusion rate for clinopyroxene may be highly variable. Theoretical studies of diffusion in silicate minerals can be used to estimate diffusion rates in different minerals [45]. Our preliminary calculations confirm that Li diffuses in olivine at about the same rate as Fe–Mg diffusion. The smaller ionic charge of Li favours faster Li diffusion than Mg, but this is counteracted by the fact that Li has an ionic radius that is larger than the ideal site radius. Calculations also confirm that Li should diffuse much faster in clinopyroxene than olivine.

6.4. Fitting the Li isotope profiles

Now that we have obtained an estimate for the diffusion rate of Li in clinopyroxene we can model our measured Li and Li isotope profiles. Li concentration profiles are fitted using a least squares method that produces values for time and C_S/C_0. These values are then used to generate Li isotope profiles using the numerical model; thus the only free variable is the δ^7Li value of the rim. The model results are remarkably consistent with our data (Fig. 9). Although the clinopyroxene in lava 95.11.14.10 was used to calibrate the Li diffusion rate in clinopyroxene, our model also fits the data for sample 95.11.13.8 very well. Encouragingly, the fitting procedure produces δ^7Li values for the rims that are within error of the matrix that we measured by ion-microprobe; this strongly supports an open-system model.

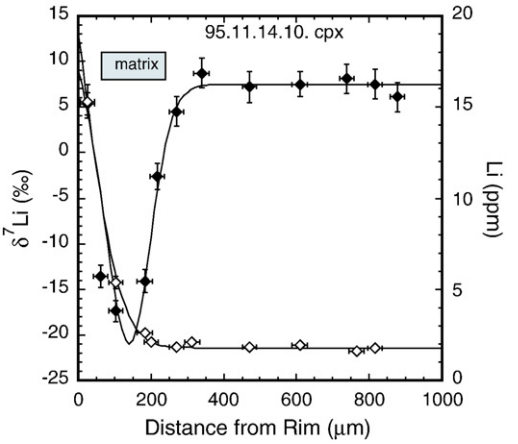

Fig. 9. Best fit diffusion profiles (solid lines) that reproduces the measured profiles of Li concentration (open diamonds) and δ^7Li (solid diamonds) for clinopyroxene in sample 95.14.11.10. The model is generated using methods described in the text. The δ^7Li composition of the matrix for this particular sample is represented by the grey box and is similar to the rim δ^7Li calculated in the model.

7. Implications

Li diffusion in clinopyroxene is a potentially powerful geospeedometer for processes that occur over a few to hundreds of days [23]. Our study indicates that the absolute diffusion rate needs to be better constrained. Nevertheless, our new data have important implications for interpreting the Li isotope systematics of magmatic rocks.

Whole-rock Li isotope analyses of NGG lavas indicated that δ^7Li did not correlate with elements that are added to the mantle wedge from the slab, even though they are enriched in elemental Li relative to MORB [28]. The ion-microprobe data reported in this study indicate that the whole-rock Li isotope data actually reflect a mixture of (1) matrix with high Li concentration and high δ^7Li and (2) phenocrysts or xenocrysts with low Li concentration and low δ^7Li value. Integrating the δ^7Li profiles for the NGG clinopyroxenes to give the δ^7Li value of the bulk phenocryst reveals that the phenocrysts can be up to 5–10‰ lighter than their matrix. If the NGG lavas comprise 30% phenocrysts, then the δ^7Li value of the whole-rock is 1–3‰ lower than the δ^7Li value of the mantle source. This effectively wipes out any effect of addition of Li (that has high δ^7Li) from the slab to the mantle wedge [1,6,9]; 'true' mantle δ^7Li values are probably only recorded by glassy phenocryst-poor lavas. We note that much of the Li isotope data published for

subduction zone lavas are from sub-aerial arc lavas that are commonly porphyritic. Thus, it is impossible to evaluate whether such lavas actually record a subduction zone signature without high-resolution studies.

Whether any subduction signature can be carried by melts across the mantle wedge depends on the melt transport mechanism, but the speed of Li diffusion means that melt equilibration with the mantle is highly likely. Melt equilibration in the mantle wedge has already been invoked to explain the overlap in δ^7Li between MORB and arc lavas [46]; this study thus lends support to this argument, but also suggests that extreme Li isotopic signatures may be 'smoothed out' during melt transport anywhere within the mantle.

Finally, the large difference in rate of Li diffusion in clinopyroxene and olivine results in Li isotope disequilibrium between these two phases during the initial stages of melt/mineral interaction. Mantle xenoliths interact with their host lavas during xenolith transport and shifts in δ^7Li of several ‰ can occur during this time (~a few days). Diffusional effects could therefore explain the common observation of lighter δ^7Li values in clinopyroxene relative to olivine [12,20], and the very low δ^7Li values of mantle xenoliths from Japan and eastern Russia [10]. Crucially, our study indicates that Li isotope data for hand-picked mantle clinopyroxenes are more likely to record information about melt/mineral interaction than primary mantle signatures.

8. Conclusions

Profiles of Li isotope ratios and Li concentrations across clinopyroxene phenocrysts in NGG lavas are consistent with diffusion-dominated modification of the mineral grains. The clinopyroxenes have a rim that is enriched in Li by 2–8 times that of the grain interior and this concentration gradient drives ^{6}Li into the mineral producing a zone with very low δ^7Li (as low as −20‰). With time, the δ^7Li trough broadens and migrates to the core of the mineral and the minimum value of the δ^7Li trough decreases. This sequence of events can be successfully reproduced by numerical modelling of Li diffusion within a sphere.

Fe–Mg diffusion profiles for co-existing olivines allow us to calculate residence times and to quantify Li diffusion rates. To this end, we show that both Li isotope and Fe-Mg profiles yield crystal residence times of between 13 and 148 days. Furthermore, we calculate that Li diffusion is some 4–8 times slower in olivine and 20–30 times faster in clinopyroxene than Fe–Mg diffusion in olivine. Finally, we demonstrate that ^{6}Li diffuses ~3% faster than ^{7}Li in silicate minerals consistent with previously reported Li isotope diffusion rates in silicate melts.

Li diffusion in silicate minerals means that Li isotope fractionation can be used as a geospeedometer for timescales of a few to hundreds of days. However, Li diffusion will also modify the composition of porphyritic lavas, mantle clinopyroxenes and melts during melt migration in a matter of days; this can obliterate primary Li isotope signatures.

Acknowledgements

Ion-microprobe studies at Edinburgh were supported by an NERC grant to RHJ, IJP, NWR and SJH. SJH was supported by a NERC studentship. Simone Kasemann is thanked for her invaluable help in collecting the ion-microprobe data. Sample collection in the Solomon Islands was supported by an ARC grant to Richard Arculus at the Australian National University. Careful reviews by Craig Lundstrom and Paul Tomascak have helped us produce a clearer manuscript. Ray MacDonald is thanked for reading an earlier version of this paper.

Appendix A. Supplementary data

Supplementary data associated with this article can be found, in the online version, at doi:10.1016/j.epsl.2007.03.023.

References

[1] P.B. Tomascak, Developments in the understanding and applications of lithium isotopes in the Earth and planetary sciences, in: C. Johnson, B. Beard, F. Albarede (Eds.), Geochemistry of Non-Traditional Isotope Systems, MSA Rev. Mineral. Geochem., vol. 55, 2004, pp. 153–195.

[2] L.H. Chan, J.M. Edmond, Variation of lithium isotope composition in the marine environment, Geochim. Cosmochim. Acta 52 (1988) 1711–1717.

[3] G.D. Flesch, A.R. Anderson Jr., H.J. Svec, A secondary isotopic standard for ^{6}Li/^{7}Li determinations, Int. J. Mass Spectrom. Ion Process. 12 (1973) 265–272.

[4] F.Z. Teng, W.F. McDonough, R.L. Rudnick, C. Dalpe, P.B. Tomascak, S. Gao, B.W. Chappell, Lithium isotopic composition and concentration of the upper continental crust, Geochim. Cosmochim. Acta 68 (2004) 4167–4178.

[5] R.L. Rudnick, P.B. Tomascak, H.B. Njo, L.R. Gardner, Extreme lithium isotopic fractionation during continental weathering revealed in saprolites from South Carolina, Chem. Geol. 212 (2004) 45–57.

[6] T.R. Elliott, A. Jeffcoate, C. Bouman, The terrestrial Li isotope cycle: light-weight constraints on mantle convection, Earth Planet. Sci. Lett. 220 (2004) 231–245.

[7] L.H. Chan, J.M. Edmond, J.M. Thompson, K. Gillis, Lithium isotopic composition of submarine basalts-implications for the

lithium cycle in the oceans, Earth Planet. Sci. Lett. 108 (1992) 151–160.
[8] S. DeCitre, E. Deloule, L. Reisberg, R. James, P. Agrinier, C. Mevel, Behavior of Li and its isotopes during serpentinization of oceanic peridotites, Geochem. Geophys. Geosyst. (2002), doi:10.1029/2001GC000178.
[9] T. Moriguti, E. Nakamura, Across-arc variation of Li isotopes in lavas and implications for crust/mantle recycling at subduction zones, Earth Planet. Sci. Lett. 163 (1998) 167–174.
[10] Y. Nishio, S. Nakai, J. Yamamoto, H. Sumino, T. Matsumoto, V.S. Prikhod'ko, S. Arai, Lithium isotopic systematics of the mantle-derived ultramafic xenoliths: implications for EM1 origin, Earth Planet. Sci. Lett. 217 (2004) 245–261.
[11] R. Brooker, J. Blundy, R. James, Trace element and Li isotopic systematics in Zabargad peridotites: evidence of ancient subduction processes in the Red Sea mantle, Chem. Geol. 212 (2004) 179–204.
[12] H.-M. Seitz, G.P. Brey, Y. Lahaye, S. Durali, S. Weyer, Lithium isotope signatures of peridotite xenoliths and isotopic fractionation at high temperature between olivine and pyroxenes, Chem. Geol. 212 (2004) 163–177.
[13] H.-M. Seitz, A.B. Woodland, The distribution of lithium in peridotitic and pyroxenitic mantle lithologies-an indicator of magmatic and metasomatic processes, Chem. Geol. 166 (2000) 47–64.
[14] F.M. Richter, A.M. Davis, D.J. DePaolo, E.B. Watson, Isotope fractionation by chemical diffusion between molten basalt and rhyolite, Geochim. Cosmochim. Acta 67 (2003) 3905–3923.
[15] F.M. Richter, Y. Liang, A.M. Davis, Isotopic diffusion by diffusion in molten oxides, Geochim. Cosmochim. Acta 63 (1999) 2853–2861.
[16] C.C. Lundstrom, M. Chaussidon, A.T. Hsui, P. Kelemen, M. Zimmerman, Observations of Li isotopic variations in the Trinity Ophiolite: evidence for isotopic fractionation during mantle melting, Geochim. Cosmochim. Acta 69 (2005) 735–751.
[17] P. Beck, M. Chaussidon, J.A. Barrat, P. Gillet, M. Bohn, Diffusion induced Li isotopic fractionation during cooling of magmatic rocks: the case study of pyroxene phenocrysts from nakhlite meteorites, Geochim. Cosmochim Acta 70 (2006) 4813–4825.
[18] A.B. Jeffcoate, T. Elliott, S.A. Kasemann, D. Ionov, K. Cooper, Li isotope fractionation in peridotites and mafic melts, Geochim. Cosmochim. Acta 71 (2007) 202–218.
[19] S. Aulbach, R.L. Rudnick, Origins of non-equilibrium lithium isotope fractionation in xenolithic peridotite minerals, Geochim. Cosmochim. Acta 70 (2006) A25.
[20] R.L. Rudnick, D.A. Ionov, Lithium elemental and isotopic disequilibrium in minerals from peridotite xenoliths from far-east Russia: product of recent melt/fluid-rock reaction, Earth Planet. Sci. Lett. 256 (2007) 278–293.
[21] C.C. Lundstrom, An experimental investigation of the diffusive infiltration of alkalis into partially molten peridotite: implications for mantle melting processes, Geochem. Geophys. Geosyst. 4 (2003) (2001GC000224).
[22] B.J. Giletti, T.M. Shanahan, Alkali diffusion in plagioclase feldspar, Chem. Geol. 139 (1997) 3–20.
[23] L.A. Coogan, S.A. Kasemann, S. Chakraborty, Rates of hydrothermal cooling of new oceanic upper crust derived from lithium-geospeedometry, Earth Planet. Sci. Lett. 240 (2005) 415–424.
[24] M.G. Petterson, T. Babbs, C.R. Neal, J.J. Mahoney, A.D. Saunders, R.A. Duncan, D. Tolia, R. Magu, C. Qopoto, H. Mahoa, D. Natogga, Geological-tectonic framework of Solomon Islands, SW Pacific: crustal accretion and growth within an intra-oceanic setting, Tectonophys 301 (1999) 35–60.
[25] K.G. Cox, J.D. Bell, A crystal fractionation model for the basaltic rocks of the New Georgia Group, British Solomon Islands, Contrib. Mineral. Petrol. 37 (1972) 1–13.
[26] W.R. Ramsey, A.J. Crawford, J.D. Foden, Field setting, mineralogy, chemistry, and genesis of arc picrites, Contrib. Mineral. Petrol. 88 (1984) 386–402.
[27] A. Rohrbach, S. Schuth, C. Ballhaus, C. Münker, S. Matveev, C. Qopoto, Petrological constraints on the origin of arc picrites, New Georgia Group, Solomon Islands, Contrib. Mineral. Petrol. 149 (2005) 685–698.
[28] S.J. Hammond, Ph.D. Thesis, The Open University, UK, 2006.
[29] A.V. McGuire, C.A. Francis, M.D. Dyar, Mineral standards for electron microprobe analysis of oxygen, Am. Mineral. 77 (1992) 1087–1091.
[30] S. Kasemann, A.B. Jeffcoate, T. Elliott, Lithium isotope composition of basaltic glass reference material, Anal. Chem. 77 (2005) 5251–5257.
[31] M. Channon, D.R. Bell, R.L. Hervig, P.R. Buseck, Isotopic composition of lithium in the Allende meteorite, LPSC 38 (2007) 1877.
[32] J. Crank, The Mathematics of Diffusion, Oxford University Press, 1976.
[33] G.D. Smith, Numerical Solutions of Partial Differential Equations: Finite Difference Methods, 3rd ed. Oxford University Press, 1985.
[34] F. Albarede, Introduction to Geochemical Modeling, Cambridge University Press, 1995.
[35] K.R. Ludwig, User's manual for Isoplot/Ex version 2.2. A geochronological toolkit for microsoft excel, Berkeley Geochronology Centre Special Publication, 2000, pp. 1–53.
[36] A.J.G. Jurewicz, E.B. Watson, Cations in olivine, Part 2. Diffusion in olivine xenocrysts, with applications to petrology and mineral physics, Contrib. Mineral. Petrol. 99 (1988) 186–201.
[37] G. Gaetani, E.B. Watson, Open system behavior of olivine-hosted melt inclusions, Earth Planet. Sci. Lett. 183 (2000) 27–41.
[38] S. Chakrobrty, Rates and mechanisms of Fe–Mg interdiffusion in olivine at 980°–1300 °C, J. Geophys. Res. 102 (1997) 12317–12331.
[39] P.L. Roeder, R.F. Emslie, Olivine-liquid equilibrium, Contrib. Mineral. Petrol. 29 (1970) 275–289.
[40] R.N. Thompson, S.A. Gibson, Transient high temperatures in mantle plume heads inferred from magnesian olivines in Phanerozoic picrites, Nature 407 (2000) 502–506.
[41] V.C. Kress, I.S.E. Carmichael, The compressibility of silicate liquids containing Fe_2O_3 and the effect of composition, temperature, oxygen fugacity and pressure on their redox states, Contrib. Mineral. Petrol. 108 (1991) 82–92.
[42] R.T. Helz, C.R. Thornber, Geothermometry of Kilauea Iki lava lake, Hawaii, Bull. Volcanol. 37 (1987) 651–668.
[43] R.R. Loucks, A precise olivine-augite Mg–Fe-exchange geothermometer, Contrib. Mineral. Petrol. 125 (1996) 140–150.
[44] D.J. Morgan, S. Blake, N.W. Rogers, B. DeVivo, G. Rolandi, R. MacDonald, C.J. Hawkesworth, Time scales of crystal residence and magma chamber volume from modelling of diffusion profiles in phenocrysts: Vesuvius 1944, Earth Planet. Sci. Lett. 222 (2004) 933–946.
[45] J.A. van Orman, T.L. Grove, N. Shimizu, Rare element diffusion in diopside: influence of temperature, pressure and ionic radius and an elastic model for diffusion in silicates, Contrib. Mineral. Petrol. 141 (2001) 687–703.
[46] P.B. Tomascak, E. Widom, L.D. Benton, S.L. Goldstein, J.G. Ryan, The control of lithium budgets in island arcs, Earth Planet. Sci. Lett. 196 (2002) 227–238.